

Short communication

## Crystal structure of a new $\text{Mo}_{10}\text{Ni}_3\text{C}_3\text{B}$ phase

T.N. Vershinina<sup>a,\*</sup>, A.O. Boev<sup>a</sup>, M.B. Ivanov<sup>b</sup><sup>a</sup> Belgorod National Research University, Pobedy Street 85, Belgorod, 308015, Russian Federation<sup>b</sup> S7 R&D Center, Vostochnaya 5, M4 Technopark, Leninskiye Gorki, Moscow Region, 142712, Russian Federation

## ARTICLE INFO

## Keywords:

Boride based cermet  
X-ray diffraction  
DFT  
Crystal structure

## ABSTRACT

A new  $\text{Mo}_{10}\text{Ni}_3\text{C}_3\text{B}$  phase was synthesized during the liquid phase sintering of cermet  $\text{Mo}_2\text{NiB}_2$ –Ni doped with carbon. The crystal structure of this phase has been determined by X-ray diffraction analysis and density functional theory calculations. The structure refinement indicates that a new phase has space group  $P6_3/mmc$  (Pearson symbol hP34) and lattice parameters  $a = 7.8089 \text{ \AA}$ ,  $c = 7.8712 \text{ \AA}$ . Atomic coordinates of all elements are determined.

Cermets on the base of Mo–Ni–B and Mo–Fe–B systems, in which boride  $\text{Mo}_2\text{NiB}_2$  or  $\text{Mo}_2\text{FeB}_2$  is the hard phase, and solid solution on the base of Ni or Fe acts as a binder phase, show good mechanical properties, excellent corrosion and wear resistance [1–4], high resistance to molten metals [5]. These cermets are of interest in the sense that their operating characteristics comparable to those of tungsten carbide-based hard alloys. But at the same time, the estimated cost of raw materials for their manufacture is significantly lower.  $\text{Mo}_2\text{NiB}_2$  and  $\text{Mo}_2\text{FeB}_2$  cermets have been successfully applied as materials for the manufacture of parts of injection molding machines and dies for copper extrusion [6], as various components for aluminum casting [7].

Despite more than thirty years of research the precise mechanism of improvements of mechanical properties of  $\text{Mo}_2\text{NiB}_2$  based cermets has not been fully understood to date. Nevertheless, it is obvious that the mechanical properties of  $\text{Mo}_2\text{NiB}_2$ –Ni cermets are strongly affected by the microstructure and phase composition. The research works available in the literature are aimed at studying the effect of doping with chromium and vanadium [3,8,9] and the Mo/B ratio [3] on the structural-phase state of  $\text{Mo}_2\text{NiB}_2$ –Ni system cermets. The purposeful doping with carbon has not been previously considered. It was found only in one work that carbon and fluorine were introduced into the initial components during the ball-milling process as a result of the contact of the powders with a milling pot [10]. A new phase formed in the  $\text{Mo}_2\text{NiB}_2$ –Ni cermet during further sintering, but authors could not determine it because of low volume fraction and designated it as Mo–Ni.

This paper presents the results of analysis of the crystal structure of the new phase, which was synthesized in the Mo–Ni–B–C system during liquid phase reaction sintering. The crystal structure of this phase has been determined by X-ray diffraction analysis and density functional

theory calculations.

High purity powders of molybdenum, nickel and boron carbide ( $\text{B}_4\text{C}$ ) were used as raw materials for production of cermet sample with a chemical composition (wt.%) 59.8Mo–35.2Ni–3.9B–1.1C. Green compact with diameter 22 mm and height of 8 mm was produced by axial pressing at 100 MPa. Compacted sample was sintered in vacuum  $1.3 \cdot 10^{-2} \text{ Pa}$  at  $1320 \text{ }^\circ\text{C}$ . For metallographic examination, sample was prepared by a two-step polishing procedure using a rotary polishing machine LaboPol-5 (Struers): first grinding with silicon carbide paper, then grinding with diamond suspension on a polishing cloth. Scanning electron microscopy (SEM) investigations (backscattered mode) were carried out in Quanta 600FEG equipped with a system for energy dispersive spectrometry (EDS).

The X-ray diffraction (XRD) analysis was performed at room temperature using ARL X'TRA diffractometer with the  $\text{Cu-K}\alpha$  radiation. Diffraction patterns were refined by using a Rietveld extended program Maud [11].

To determine optimized atomic structures and their total energies we use density functional theory (DFT) [12] within projected augmented wave (PAW) formalism [13], generalized gradient approximation (GGA) of Perdew Burke-Ernzerhof (PBE) functional [14] using the Vienna ab initio simulation package (VASP) [15] through management package SIMAN [16]. The kinetic energy cutoff of 350 eV and the Fermi-level smearing width of 0.2 eV are chosen. We use nickel, molybdenum, carbon and boron PAW-pseudopotentials with  $3d^8 4s^2$ ,  $4d^5 5s^1$ ,  $2s^2 2p^2$ ,  $2s^2 2p^1$  valence electrons respectively. To obtain optimized geometry we relax atomic positions and supercell volume until the maximum force acting on atoms is less than  $25 \text{ meV/\AA}$  using the conjugate-gradient method, which is sufficient to maintain a balance between accuracy

\* Corresponding author.

E-mail address: [vershinina@bsu.edu.ru](mailto:vershinina@bsu.edu.ru) (T.N. Vershinina).

and CPU time usage [17]. The formation energy was calculated by using the equation:  $E_f = E(N) - \sum_i \mu_i n_i$ , where  $E(N)$  is energy of supercell consisting of  $N$  atoms,  $\mu$  is a chemical potential and  $n$  is a number of  $i$ -element in the supercell. Chemical potentials of Ni, Mo, C and B were taken from the DFT database [18].

Two types of stability are distinguished in the literature: thermodynamic and dynamic [19–21]. But to determine the optimized structure in agreement with X-Ray diffraction data, it is sufficient to determine only the thermodynamic stability of a new phase by calculation of formation energy using DFT method.

Fig. 1 shows the microstructure of  $\text{Mo}_2\text{NiB}_2$ -Ni cermet doped with carbon. As can be seen, three phases are present in the structure: a solid solution based on nickel (dark phase), boride  $\text{Mo}_2\text{NiB}_2$  (dark gray phase) and a previously unknown phase (light gray phase). Analysis of the element composition showed that an atomic ratio  $\text{Mo}:\text{Ni} \approx 9:3$  corresponds to the detected phase. An X-ray diffraction pattern of the obtained sample (Fig. 2) revealed a set of peaks that could not be decrypted using existing crystallographic databases. None of the phases shown in the triple-phase diagrams  $\text{Mo-Ni-C}$ ,  $\text{Mo-Ni-B}$ ,  $\text{Mo-C-B}$ ,  $\text{Ni-C-B}$  corresponded to the obtained set of peaks. In this regard, we had proposed that during sintering the formation of phase, which simultaneously included all four elements (molybdenum, nickel, carbon, and boron) has occurred.

It was found that the positions of the undecrypted peaks on the X-ray diffraction pattern coincide with the positions of the peaks of the  $\text{W}_9\text{Co}_3\text{C}_4$  phase with hexagonal crystal lattice  $P6_3/mmc$  (Space group 194) [22]. Therefore, this lattice was taken as the basis for the refining of a new phase crystal lattice. DFT calculation was carried out to determine the equilibrium positions of molybdenum, nickel, carbon and boron atoms (Table 1). It was used a set of 32-node supercells (double unit cell) including a twelve different combination of  $\text{Mo-Ni-C-B}$  atoms ( $\text{Mo}_9\text{Ni}_3\text{C}_3\text{B}$ -type crystal lattice). The set consists of three stoichiometric configurations with different  $\text{Mo-Ni}$  distribution, three configurations with different content of C and B and three configurations with the substitution of molybdenum with nickel and vice versa. Calculated formation energies and supercell volumes were estimated (Table 1). As can be seen, the most stable atomic configuration for 32-node supercells corresponds to  $\text{Mo}_{18}\text{Ni}_6\text{C}_6\text{B}_2$  (1) configuration. We used a DFT obtained atomic positions of this structure (Table 2) as a state for calculation of theoretical XRD profile. Weighted profile factor  $R_{\text{wp}}$  (discrepancy index in the Rietveld analysis) for the case of  $\text{Mo}_9\text{Ni}_3\text{C}_3\text{B}$ -type crystal lattice is 9.95%. Nevertheless, in the process of fitting of the theoretical XRD profile to the experimental one a mismatch between intensities of several observed and calculated peaks was found (Fig. 3a).

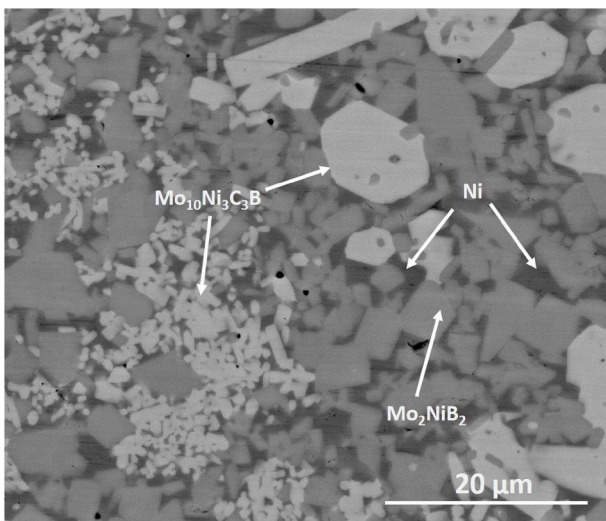


Fig. 1. Microstructure of  $\text{Mo}_2\text{NiB}_2$ -Ni cermet doped with carbon.

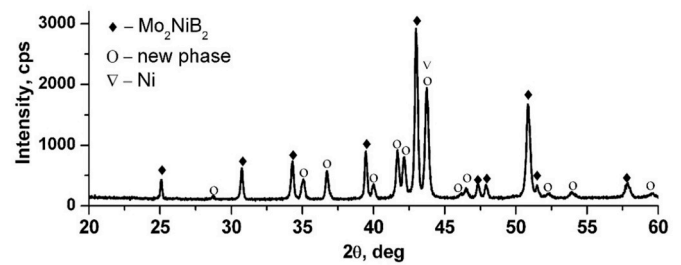


Fig. 2. XRD pattern of  $\text{Mo}_2\text{NiB}_2$ -Ni cermet doped with carbon.

Table 1

DFT calculated formation energies (in eV) of supercells with different configurations of  $\text{Mo}_9\text{Ni}_3\text{C}_3\text{B}$ -type and  $\text{Mo}_{10}\text{Ni}_3\text{C}_3\text{B}$ -type phases.

$\text{Mo}_9\text{Ni}_3\text{C}_3\text{B}$ -type			$\text{Mo}_{10}\text{Ni}_3\text{C}_3\text{B}$ -type		
Composition	$E_f$ , eV	$V$ , Å <sup>3</sup>	Composition	$E_f$ , eV	$V$ , Å <sup>3</sup>
Stoichiometric					
$\text{Mo}_{18}\text{Ni}_6\text{C}_6\text{B}_2$ (1)	-0.46	405.34	$\text{Mo}_{20}\text{Ni}_6\text{C}_6\text{B}_2$ (1)	-5.88	420.79
$\text{Mo}_{18}\text{Ni}_6\text{C}_6\text{B}_2$ (2)	3.85	409.49	$\text{Mo}_{20}\text{Ni}_6\text{C}_6\text{B}_2$ (2)	2.93	433.25
$\text{Mo}_{18}\text{Ni}_6\text{C}_6\text{B}_2$ (3)	1.38	406.53	$\text{Mo}_{20}\text{Ni}_6\text{C}_6\text{B}_2$ (3)	-1.80	425.25
Boron partially substituted					
$\text{Mo}_{18}\text{Ni}_6\text{C}_2\text{B}_6$	2.55	420.68	$\text{Mo}_{20}\text{Ni}_6\text{C}_2\text{B}_6$	-3.94	430.71
Boron fully substituted					
$\text{Mo}_{18}\text{Ni}_6\text{B}_8$	0.89	419.52	$\text{Mo}_{20}\text{Ni}_6\text{B}_8$	-5.76	433.60
Carbon fully substituted					
$\text{Mo}_{18}\text{Ni}_6\text{C}_8$	1.55	404.72	$\text{Mo}_{20}\text{Ni}_6\text{C}_8$	-3.82	417.68
Mo-substituted					
$\text{Mo}_{19}\text{Ni}_5\text{C}_2\text{B}_6$	-0.50	409.85	$\text{Mo}_{21}\text{Ni}_5\text{C}_2\text{B}_6$	-4.78	426.28
$\text{Mo}_{20}\text{Ni}_4\text{C}_2\text{B}_6$	-0.65	414.05	$\text{Mo}_{22}\text{Ni}_4\text{C}_2\text{B}_6$	-4.33	432.21
$\text{Mo}_{21}\text{Ni}_3\text{C}_2\text{B}_6$	-0.25	419.05	$\text{Mo}_{23}\text{Ni}_3\text{C}_2\text{B}_6$	-3.57	437.27
Ni-substituted					
$\text{Mo}_{17}\text{Ni}_7\text{C}_2\text{B}_6$	0.63	401.33	$\text{Mo}_{19}\text{Ni}_7\text{C}_2\text{B}_6$	-4.46	416.86
$\text{Mo}_{16}\text{Ni}_8\text{C}_2\text{B}_6$	1.14	397.16	$\text{Mo}_{18}\text{Ni}_8\text{C}_2\text{B}_6$	-3.57	413.22
$\text{Mo}_{15}\text{Ni}_9\text{C}_2\text{B}_6$	1.98	392.66	$\text{Mo}_{17}\text{Ni}_9\text{C}_2\text{B}_6$	-2.57	409.54

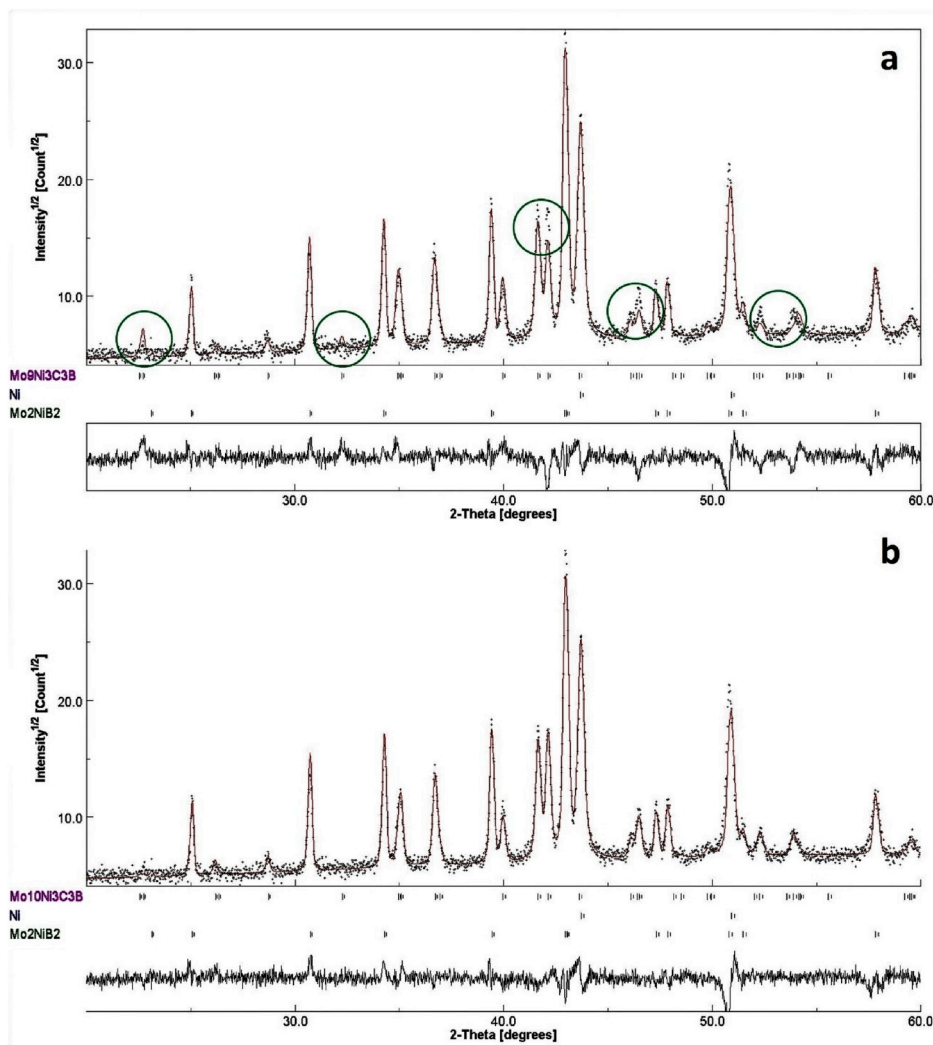
It is known that several factors contribute to the change in the ratios of the diffraction peaks intensities, one of which is the structural factor  $F(HKL)$ . The value of the  $F(HKL)$  for various crystallographic planes depends on the type of atoms entering the crystal lattice and its basis. Thus, in the subsequent refinement, the possibility of additional Mo atom at the  $2a$  position was tested. This improved the agreement between experimental and theoretical profiles, to give  $R_{\text{wp}} = 7.77\%$  (Fig. 3b). The double unit cell of this phase accounts for 20 molybdenum atoms, 6 nickel atoms, 6 carbon atoms and 2 boron atoms. Therefore, the compound formula can be defined as  $\text{Mo}_{10}\text{Ni}_3\text{C}_3\text{B}$ . As shown by numerical estimates (Table 1), a significant decrease in the formation energy is observed for  $\text{Mo}_{10}\text{Ni}_3\text{C}_3\text{B}$ -type crystal structure in comparison with the  $\text{Mo}_9\text{Ni}_3\text{C}_3\text{B}$ -type.

As for the previous  $\text{Mo}_9\text{Ni}_3\text{C}_3\text{B}$  crystal lattice, for the new  $\text{Mo}_{10}\text{Ni}_3\text{C}_3\text{B}$  version the effect of the position of the molybdenum and nickel atoms, carbon and boron on the phase formation energy was evaluated. It was found that the equilibrium crystal lattice contains Mo, Ni, C and B atoms with coordinates which are given in Table 3. The lowest formation energy corresponds to a state containing both carbon and boron. For the configuration  $\text{Mo-Ni-C}$ , a substantial increase in  $E_f$  is observed. It should be noted, that the configuration in which carbon is completely absent corresponds to the formation energy, which only slightly exceeds the formation energy of the  $\text{Mo}_{10}\text{Ni}_3\text{C}_3\text{B}$  phase, but the crystal lattice parameters differ significantly from the experimental values (Table 4). That is, it can be assumed that this new phase can exist only in the case of the  $\text{Mo-Ni-B-C}$  quaternary system and, therefore, it was not detected in the  $\text{Mo-Ni-B}$  and  $\text{Mo-Ni-C}$  ternary phase diagrams.

The lattice parameters calculated according to XRD data and obtained by numerical methods differ from each other. This is primarily because of the replacement of individual atoms that could take place in the real material. Consequently, this replacement led to a change in the

**Table 2**DFT obtained atomic coordinates, Wyckoff symbols, site occupancy factor for  $\text{Mo}_9\text{Ni}_3\text{C}_3\text{B}$ -type crystal lattice ( $P6_3/mmc$ ,  $a = 7.7514 \text{ \AA}$ ,  $c = 7.7898 \text{ \AA}$ ,  $Z = 2$ ).

No	Site notation	Atom	Multiplicity	Wyckoff	Site symmetry	x	y	z	Occupancy
1	Ni	Ni	6	h	mm2	0.8964	0.7928	1/4	1.0
2	Mo1	Mo	12	k	.m.	0.1985	0.3970	0.0664	1.0
3	Mo2	Mo	6	h	mm2	0.5509	0.1019	1/4	1.0
4	C	C	6	g	.2/m.	1/2	0	0	1.0
5	B	B	2	c	-6m2	1/3	2/3	1/4	1.0

**Fig. 3.** Rietveld refinement with the software package Maud: a – for the case of  $\text{Mo}_9\text{Ni}_3\text{C}_3\text{B}$ ; b – for the case of  $\text{Mo}_{10}\text{Ni}_3\text{C}_3\text{B}$ .**Table 3**DFT obtained atomic coordinates, Wyckoff symbols, site occupancy factor for  $\text{Mo}_{10}\text{Ni}_3\text{C}_3\text{B}$ -type crystal lattice ( $P6_3/mmc$ ,  $a = 7.8265 \text{ \AA}$ ,  $c = 7.9243 \text{ \AA}$ ,  $Z = 2$ ).

No	Site notation	Atom	Multiplicity	Wyckoff	Site symmetry	x	y	z	Occupancy
1	Ni	Ni	6	h	mm2	0.8885	0.7770	1/4	1.0
2	Mo1	Mo	12	k	.m.	0.2011	0.4024	0.0695	1.0
3	Mo2	Mo	6	h	mm2	0.5521	0.1041	1/4	1.0
4	Mo3	Mo	2	a	-3m.	0	0	0	1.0
5	C	C	6	g	.2/m.	1/2	0	0	1.0
6	B	B	2	c	-6m2	1/3	2/3	1/4	1.0

crystal lattice parameters. It should be noted, that the random rearrangement (Table 1,  $\text{Mo}_{20}\text{Ni}_6\text{C}_6\text{B}_2$  (2) and  $\text{Mo}_{20}\text{Ni}_6\text{C}_6\text{B}_2$  (3) configurations) and substitution (Table 1, Mo-substituted and Ni-substituted configurations) of nickel atoms by molybdenum atoms and vice versa

leads to an increase in the phase formation energy.

Thus, we report on the formation of a new phase during liquid phase reactive sintering of high purity powders of molybdenum, nickel and boron carbide. Its crystal structure was determined to be hexagonal with

**Table 4**

DFT obtained lattice parameters of the most stable configurations of Mo<sub>10</sub>Ni<sub>3</sub>C<sub>3</sub>B-phase in comparison with experimental data.

Configuration	a, Å	c, Å
DFT Mo <sub>20</sub> Ni <sub>6</sub> C <sub>6</sub> B <sub>2</sub> (1)	7.8265	7.9243
DFT Mo <sub>20</sub> Ni <sub>6</sub> B <sub>8</sub>	7.8851	8.0528
Experimental	7.8089	7.8712

space group  $P6_3/mmc$  (Pearson symbol hP34) and a chemical formula is defined as Mo<sub>10</sub>Ni<sub>3</sub>C<sub>3</sub>B. The energy of formation of a new phase was calculated using the density functional theory method and it was shown, that the crystal lattice of an ordered Mo<sub>10</sub>Ni<sub>3</sub>C<sub>3</sub>B phase corresponds to the equilibrium configuration.

## References

- [1] K.-i. Takagi, Mater. Chem. Phys. 67 (2001) 214–219, [https://doi.org/10.1016/S0254-0584\(00\)00442-9](https://doi.org/10.1016/S0254-0584(00)00442-9).
- [2] M. Komai, Y. Yamasaki, K. Takagi, Solid State Phenomena, vol. 25, Trans Tech Publ, 1992, pp. 531–538. <https://doi.org/10.4028/www.scientific.net/SSP.25-26.531>.
- [3] K.-i. Takagi, Y. Yamasaki, J. Solid State Chem. 154 (2000) 263–268, <https://doi.org/10.1006/jssc.2000.8847>.
- [4] M.B. Ivanov, T.N. Vershinina, V.V. Ivanisenko, Mater. Sci. Eng. A 763 (2019) 138117, <https://doi.org/10.1016/j.msea.2019.138117>.
- [5] K. Hamashima, in: MaterialsScienceForum, vol. 426, Trans Tech Publ, 2003, pp. 2545–2550.
- [6] K.-i. Takagi, J. Solid State Chem. 179 (2006) 2809–2818, <https://doi.org/10.1016/j.jssc.2006.01.023>.
- [7] Y. Yamauchi, Y. Yata, R. Masuda, H. Kokumai, K. Hamashima, T. Yasuda, J. Jpn. Foundrymen's Soc. 6 (1994) 223–228, [https://doi.org/10.11279/ijmono.66.3\\_223](https://doi.org/10.11279/ijmono.66.3_223).
- [8] K.-i. Takagi, W. Koike, A. Momozawa, T. Fujima, Solid State Sci. 14 (2012) 1643–1647, <https://doi.org/10.1016/j.solidstatesciences.2012.05.009>.
- [9] Y. Yamasaki, M. Nishi, K.-i. Takagi, J. Solid State Chem. 177 (2004) 551–555, <https://doi.org/10.1016/j.jssc.2003.03.008>.
- [10] L. Zhang, Z. Huang, Y. Liu, Y. Shen, K. Li, Z. Cao, Z. Ren, Y. Jian, Materials 12 (2019) 1926, <https://doi.org/10.3390/ma12121926>.
- [11] L. Lutterotti, S. Matthies, H. Wenk, IUCr: Newsletter of the CPD, vol. 21, 1999.
- [12] W. Kohn, L.J. Sham, Phys. Rev. 140 (1965) A1133.
- [13] P.E. Blöchl, Phys. Rev. B 50 (1994) 17953.
- [14] J.P. Perdew, K. Burke, M. Ernzerhof, Phys. Rev. Lett. 77 (1996) 3865, <https://doi.org/10.1103/PhysRevLett.77.3865>.
- [15] G. Kresse, J. Furthmüller, Comput. Mater. Sci. 6 (1996) 15–50, [https://doi.org/10.1016/0927-0256\(96\)00008-0](https://doi.org/10.1016/0927-0256(96)00008-0).
- [16] D. Aksyonov, S. Fedotov, K. Stevenson, A. Zhugayevych, Comput. Mater. Sci. 154 (2018) 449–458, <https://doi.org/10.1016/j.commatsci.2018.07.057>.
- [17] A. Boev, D. Aksyonov, A. Kartamyshev, V. Maksimenko, I. Nelasov, A. Lipnitskii, J. Nucl. Mater. 492 (2017) 14–21, <https://doi.org/10.1016/j.jnucmat.2017.04.046>.
- [18] A. Jain, S.P. Ong, G. Hautier, W. Chen, W.D. Richards, S. Dacek, S. Cholia, D. Gunter, D. Skinner, G. Ceder, et al., Apl. Mater. 1 (2013), 011002, <https://doi.org/10.1063/1.4812323>.
- [19] Y. Pan, W.M. Guan, Exploring the novel structure, elastic and thermodynamic properties of W3Si silicides from first-principles calculations, Ceram. Int. 45 (12) (2019) 15649–15653.
- [20] Yong Pan, Chao Jin, Vacancy-induced mechanical and thermodynamic properties of B2-RuAl, Vacuum 143 (2017) 165–168.
- [21] Y. Pan, C. Jing, Y.P. Wu, The structure, mechanical and electronic properties of WSi2 from first-principles investigations, Vacuum 167 (2019) 374.
- [22] N. Schönberg, Acta Metall. 2 (1954) 837–840.